Rapid Communications

Molecular beam epitaxy growth and surface structure of $Sr_{1-x}Nd_xCuO_2$ cuprate films

Jia-Qi Fan,[1] Shu-Ze Wang,[1] Xue-Qing Yu,[1] Rui-Feng Wang,[1] Yan-Ling Xiong,[1] Can-Li Song,[1,2,*] Xu-Cun Ma,[1,2,†] and Qi-Kun Xue[1,2,3]

[1]*State Key Laboratory of Low-Dimensional Quantum Physics, Department of Physics, Tsinghua University, Beijing 100084, China*
[2]*Frontier Science Center for Quantum Information, Beijing 100084, China*
[3]*Beijing Academy of Quantum Information Sciences, Beijing 100193, China*

(Received 17 February 2020; revised manuscript received 15 April 2020; accepted 1 May 2020; published 18 May 2020)

We report on the epitaxial growth and surface structure of infinite-layer cuprate $Sr_{1-x}Nd_xCuO_2$ films on $SrTiO_3$(001) substrates by combining ozone-assisted molecular beam epitaxy and *in situ* scanning tunneling microscopy. Careful substrate temperature and flux control has been used to achieve single-phase, stoichiometric, and *c*-axis oriented films. The surface of the films is usually characterized by a mixed CuO_2 surface and gridlike superstructure. The superstructure exhibits a periodicity of 3.47 nm that corresponds to a coincidence lattice between the overlayer peroxide SrO_2 and underlying CuO_2 plane, and gives rise to a conductance spectrum that is distinct from the Mott-Hubbard band structure of CuO_2. At a higher Nd composition $x > 0.1$, a (2×2) surface characteristic of the hole-doped CuO_2 emerges, which we ascribe to the intake of apical oxygens in the intervening Sr planes.

DOI: 10.1103/PhysRevB.101.180508

Infinite-layer (IL) $ACuO_2$ (A = Ca, Sr, Ba) compounds exhibit the simplest crystal structure among cuprates, in which the major superconducting CuO_2 is alternatively separated by alkaline-earth cations along the crystallographic c axis [1]. Partial substitution of divalent A^{2+} ions by trivalent ions such as La^{3+} and Nd^{3+} leads to electron-doped superconductivity with a record transition temperature T_c of 43 K [2–4]. More remarkably, IL compounds represent a rare category of cuprate superconductors with a surface termination of the superconducting CuO_2 planes [5–7]. Given that most cuprates are terminated with non-CuO_2 charge reservoir layers upon cleaving, e.g., BiO for bismuth-based cuprates, this peculiar feature provides an unprecedented opportunity to directly characterize the superconducting CuO_2 planes by surface-sensitive experiments [8], compared to previous studies [9–11]. A systematic direct measurement of the major CuO_2 planes may help to eventually understand the microscopic mechanism of high-T_c superconductivity [3,8,12–16]. However, IL cuprates with a tetragonal structure are thermodynamically unstable. It is nearly impossible to synthesize single crystals by conventional solid state methods, and only some powder form of IL samples was obtained using high-pressure techniques [17,18].

Epitaxial films of IL cuprates can be stabilized and prepared on appropriate substrates by using pulsed laser deposition (PLD) [19–21] or the reactive molecular beam epitaxy (MBE) technique [22–25]. However, the as-grown thin films are often characterized with several competing phases, such as Sr_2CuO_3, $Sr_{14}Cu_{24}O_{41}$, and orthorhombic $SrCuO_2$ [26], as summarized in Table I. Furthermore, due to the limited solubility of trivalent ions in IL compounds, oxygen-deficient or -redundant superstructures with a relatively larger out-of-plane lattice parameter, referred to as a long-c phase, occur at elevated doping [8,19,20,22]. In this Rapid Communication, we combine ozone-assisted MBE and *in situ* scanning tunneling microscopy (STM) to solve these problems, aiming to establish growth procedures for single-phase crystalline $Sr_{1-x}Nd_xCuO_2$ (SNCO, $0.08 \leqslant x \leqslant 0.12$) thin films. We emphasize that, compared to the alternative shutter-controlled deposition, our method for composition/phase control is self-regulated, without the complicated calibration of the composition by shutter time.

The experiments were performed on a commercial ultrahigh vacuum (UHV) STM apparatus (Unisoku), connected to an ozone-assisted MBE chamber for *in situ* film growth. Nb-doped $SrTiO_3$(001) substrates were first degassed at 600 °C, and subsequently annealed at 1250 °C under UHV for 20 min to get the clean surface. Prior to film epitaxy, fluxes of all metal sources (Sr, Nd, and Cu) were precisely calibrated in sequence by using a standard quartz crystal microbalance (QCM, Inficon SQM160H). Epitaxial thin films were then prepared by the codeposition of high-purity metal sources from standard Knudsen cells under an ozone flux beam of $\sim 1.1 \times 10^{-5}$ Torr. The growth rate was 0.4 unit cells per min, and the flux ratio between Nd and Cu sources was used to calculate the nominal composition x. Polycrystalline PtIr tips were cleaned by electron-beam heating and calibrated on MBE-grown Ag/Si(111) films. Tunneling spectra were measured using a standard lock-in technique with a small bias modulation of 10 mV at 937 Hz. After *in situ* STM measurements at 78 K, the samples were taken out from the UHV chamber for x-ray diffraction (XRD) measurements using the monochromatic Cu $K\alpha 1$ radiation with a wavelength of 1.5406 Å.

*clsong07@mail.tsinghua.edu.cn
†xucunma@mail.tsinghua.edu.cn

TABLE I. Crystal structure and lattice parameters for Sr-Cu-O compounds in the thermodynamic proximity of IL cuprates.

	Space group	a (Å)	b (Å)	c (Å)	Reference
IL tetragonal $SrCuO_2$	$P4/mmm$	3.9269	$= a$	3.4346	[1]
Orthorhombic $SrCuO_2$	$Cmcm$	3.5770	16.342	3.9182	[27]
Orthorhombic Sr_2CuO_3	$Immm$	12.702	3.911	3.4990	[28]
Orthorhombic $Sr_{14}Cu_{24}O_{41}$	$Amma$	11.488	13.414	27.428	[29]
Tetragonal SrO_2	$I4/mmm$	3.55	$= a$	6.55	[30]

The growth of IL SNCO epitaxial films demands for the precise control of the substrate temperature T_{sub} and cation stoichiometry. Similar to previous reports [31], we found that tetragonal IL SNCO films start to crystallize at 500 °C and change to the orthorhombic phase above 610 °C. Thus, $T_{sub} =$ 550 °C was chosen for both good crystallinity and avoiding a high-temperature orthorhombic phase. Figure 1(a) shows the XRD patterns of as-grown films as a function of the nominal flux ratio $\lambda = (\mathrm{Sr} + \mathrm{Nd})/\mathrm{Cu}$, with a smaller Nd/Cu flux ratio of $x \leqslant 0.10$. Apparently, the IL SNCO phase coexists with the Sr-deficient spin ladder $Sr_{14}Cu_{24}O_{41}$ at a lower λ of 7.3. This is understandable because Sr has a higher vapor pressure of 1.8×10^{-2} Torr and is very volatile at $T_{sub} = 550$ °C. Meanwhile, Sr is easily oxidized in the ozone atmosphere, which reduces its effective flux during the growth. The two factors explain why a larger $\lambda \geqslant 9.4$ is required to prepare single-phase IL films, as demonstrated by the XRD spectra in Fig. 1(a). Evidently, the cation stoichiometry of SNCO is quasi-self-regulating, resembling, to some extent, the growth of GaAs and metal chalcogenides [32,33]. We note that the self-regulation of stoichiometry is somewhat limited and the IL SNCO phase forms only in a narrow window of λ. A larger λ of 16.8 converts the epitaxial films to a more thermodynamically stable Sr_2CuO_3 phase [see Fig. 1(a)].

Our STM characterization corroborates the flux-ratio-dependent phase evolution. At $\lambda = 7.3$, the chainlike surface characteristic of spin ladder $Sr_{14}Cu_{24}O_{41}(010)$ occurs [Fig. 1(b)], whereas single-phase Sr_2CuO_3 overwhelms the others under a Sr-rich condition [Figs. 1(c) and 1(d)]. A fast Fourier transform (FFT) analysis inserted in Fig. 1(d) indicates that the in-plane lattice constants are $b = 3.9 \pm 0.1$ Å and $c = 3.5 \pm 0.1$ Å, consistent with the expected value for the orthorhombic $Sr_2CuO_3(100)$ surface in Table I. The single-phase IL SNCO films are prepared at an intermediate λ and display atomically flat surfaces [Figs. 1(e)–1(g)], which are separated by a gridlike superstructure. The gridlike feature gradually becomes prominent with increasing λ and covers the whole surface at $\lambda \sim 10.5$.

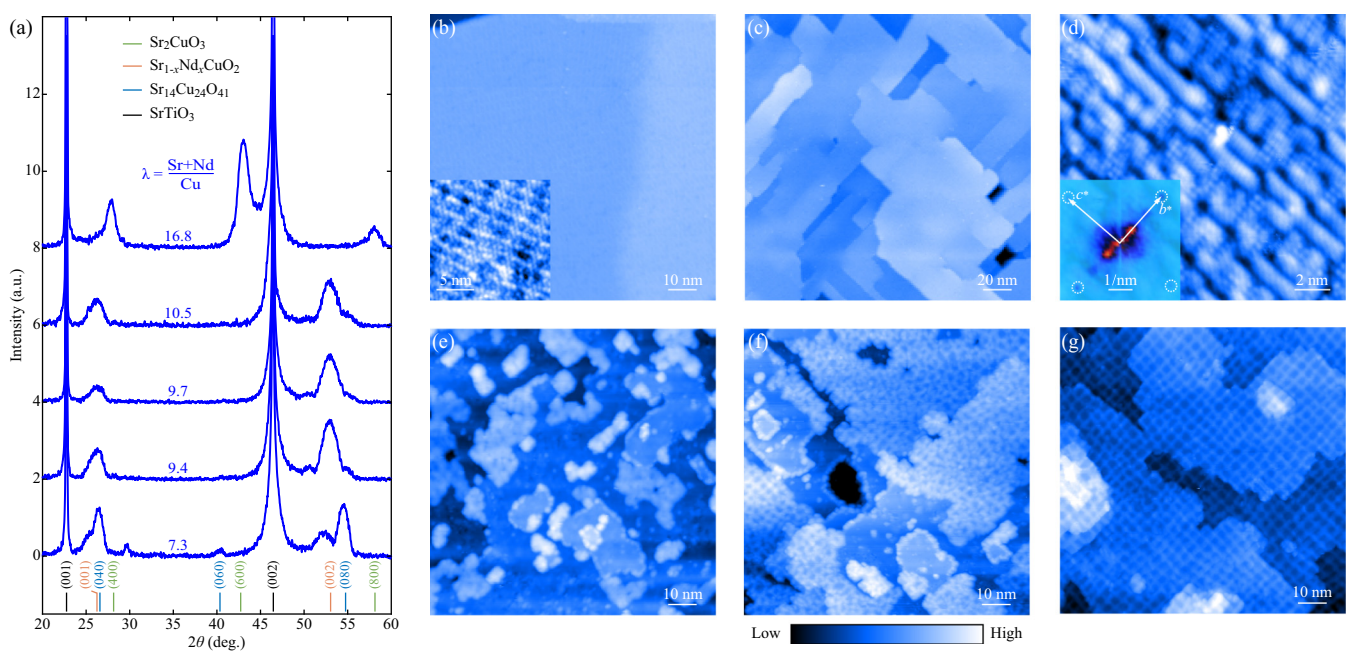

FIG. 1. (a) Representative XRD patterns of epitaxial films grown with various flux ratios $(\mathrm{Sr} + Nd)/\mathrm{Cu}$ as indicated. The color vertical bars correspond to the indexation of the crystal structure database for the referred to different phases. (b) STM topography (100 nm × 100 nm, $V = -5.5$ V, $I = 20$ pA) of spin ladder $Sr_{14}Cu_{24}O_{41}$ at a small λ of 7.3. Inserted is a zoom-in STM image of the chainlike (010) surface (20 nm × 20 nm, $V = -4.0$ V, $I = 20$ pA). (c) Large-scale STM topography (200 nm × 200 nm, $V = -4.0$ V, $I = 20$ pA) of Sr_2CuO_3 at a large λ of 16.8. (d) Atomic-resolved STM image of Sr_2CuO_3 (16 nm × 16 nm, $V = -4.5$ V, $I = 15$ pA). The inset shows the corresponding FFT image, with b^* and c^* denoting the two reciprocal lattice vectors. (e)–(g) Morphographies (100 nm × 100 nm, $I = 20$ pA) of IL SNCO cuprate films with increasing λ. The sample bias V for STM imaging is (e) 3.0 V, (f) −4.0 V, and (g) −3.5 V. The Nd composition x is 0.08 in (e) and (f) and 0.10 in (g).

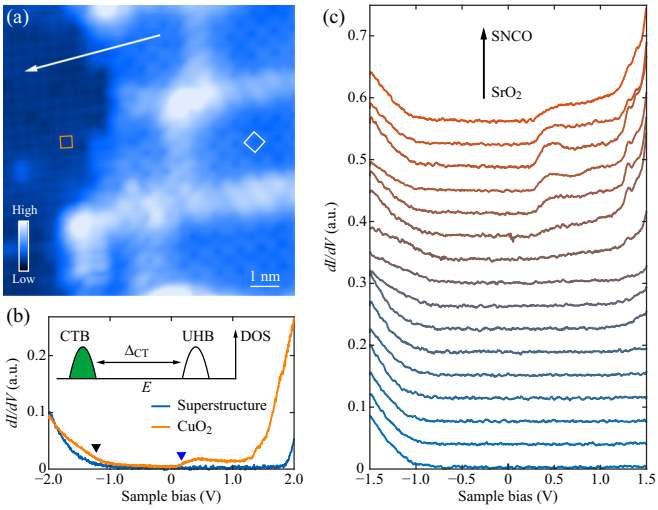

FIG. 2. (a) Atomically resolved topography (10 nm × 10 nm, $V = -2.0$ V, $I = 20$ pA) across a step edge separating the CuO_2 plane (left side) and gridlike superstructure (right side) in $Sr_{0.9}Nd_{0.1}CuO_2$. Orange and white squares denote the respective in-plane unit cells. (b) Spatially averaged tunneling spectra on CuO_2 and the gridlike superstructure. Inserted is the schematic band structure of pristine cuprates displaying the UHB (unfilled) and CTB (green). The black and blue triangles mark the onsets of CTB and UHB throughout. Set point: $V = -2.0$ V, $I = 100$ pA. (c) A series of dI/dV spectra acquired along the white arrow in (a). Set point: $V = -1.5$ V, $I = 20$ pA.

To identify the two apparently distinct surfaces of IL SNCO films, we acquire atomically resolved STM images, as illustrated in Fig. 2(a). The flat surface has a square lattice with a periodicity of ∼3.9 Å, matching well the CuO_2-terminated IL SNCO [2,8]. This is indeed supported by the site-dependent differential conductance dI/dV spectra in Fig. 2(b). On the flat surface, the tunneling dI/dV spectrum features a fundamental Mott-Hubbard band structure of the cuprate CuO_2 planes, accompanied by metalliclike states within the charge-transfer gap [8]. It is worth noting that the Fermi level E_F is closer to the upper Hubband (UHB) than the charge-transfer band (CTB), in line with the electron doping by the Nd^{3+} substitution for Sr^{2+} ions.

In contrast, the gridlike superstructure is characterized by a larger in-plane unit cell of ∼5.0 Å (marked by the white square), rotated by 45° relative to the CuO_2 unit cell in Fig. 2(a). A possible surface reconstruction of SNCO(001)-$\sqrt{2} \times \sqrt{2}R45^\circ$ could be safely excluded since the measured periodicity of ∼5.0 Å deviates substantially from the $\sqrt{2}$ times (∼5.6 Å) of the in-plane lattice constant of SNCO. Moreover, the tunneling dI/dV spectrum of the gridlike superstructure shows an extremely large band gap (∼2.8 eV) and is significantly different from that of CuO_2 plane [Fig. 2(b)]. This is confirmed by the linecut dI/dV spectra across one step edge between the gridlike superstructure and the CuO_2 surface in Fig. 2(c). These observations, together with the populated gridlike superstructure at elevated λ [Figs. 1(e)–1(g)], strongly suggest that the superstructure originates from a totally different compound, most probably linking with strontium. Tetragonal strontium peroxide SrO_2 has a lattice constant of 3.55 Å in the *a*-*b* plane (Table I) [30], coinciding with $1/\sqrt{2}$ of the measured unit cell periodicity of 5.0 Å in Fig. 2(a). In other words, the gridlike surface might

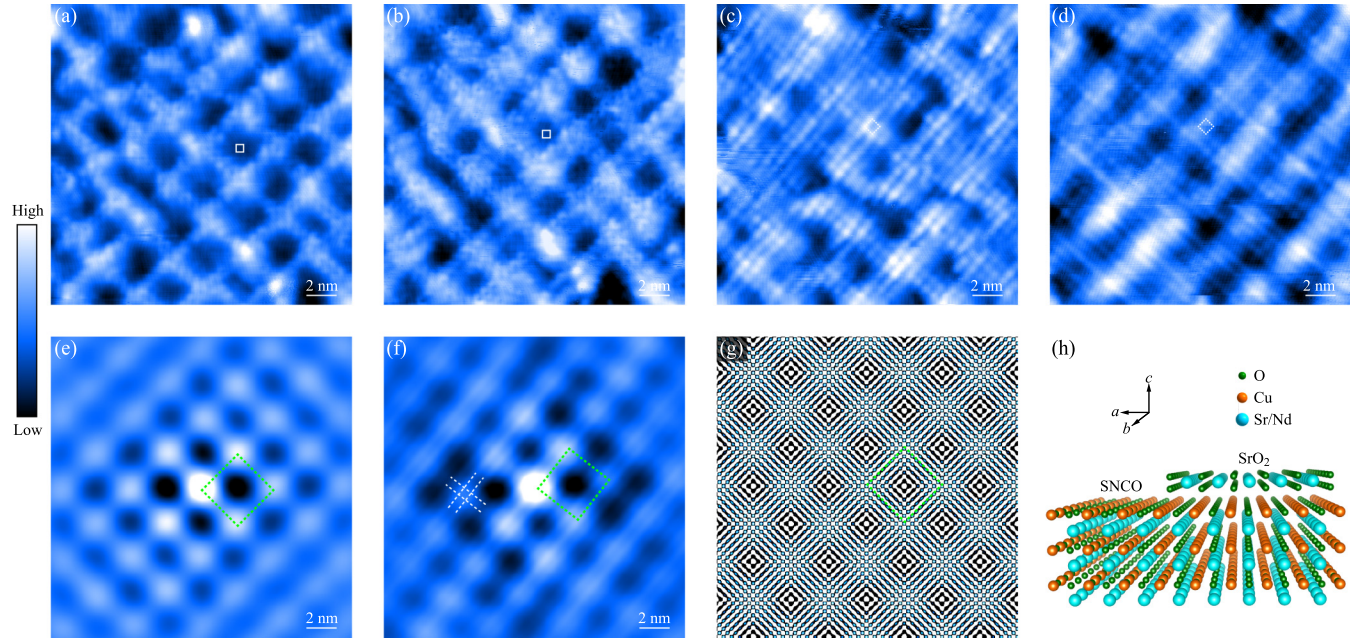

FIG. 3. (a)–(d) Bias-dependent STM images (20 nm × 20 nm, $I = 20$ pA) of the coincidence lattice between the SrO_2 overlayer and CuO_2 plane. The bias V is (a) −3.0 V, (b) −2.0 V, (c) 3.0 V, and (d) 4.0 V. Note that the surface structure alters from SrO_2(001)-$\sqrt{2} \times \sqrt{2}R45^\circ$ (solid squares) to SrO_2(001)-2 × 2 (dashed squares) as the bias polarity is reversed. (e), (f) Autocorrelation analysis of the STM images in (a) and (c), respectively. The green squares represent the unit cells of the gridlike superstructure. (g) Simulated moiré pattern between SrO_2 and CuO_2. (h) Schematic sketch of the SrO_2 overlayer on CuO_2-terminated SNCO films.

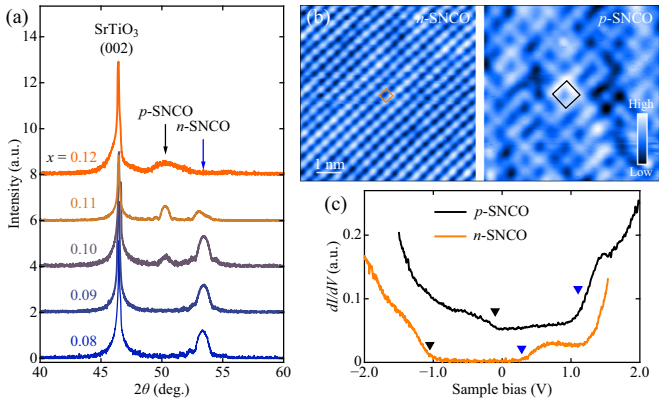

FIG. 4. (a) XRD spectra of IL SNCO films with varying x. Blue and black arrows denote the reflection peaks from n- and p-SNCO, respectively. (b) STM topographies (7 nm × 7 nm, $I = 20$ pA) of coexisting n-SNCO (left panel, $V = -1.5$ V) and p-SNCO films (right panel, $V = -3.0$ V) at $x = 0.12$. The unit cells outlined by colored squares become doubled in size for p-SNCO as compared with n-SNCO. (c) Comparison between tunneling dI/dV spectra on n-SNCO ($V = -2.0$ V, $I = 100$ pA) and p-SNCO films ($V = -1.5$ V, $I = 100$ pA).

correspond to SrO_2 in nature, which exhibits an enlarged surface structure, i.e., $SrO_2(001)$-$\sqrt{2} \times \sqrt{2}R45^\circ$. Considering that no excess phase other than IL SNCO is found in the bulk-sensitive XRD spectra at intermediate λ [Fig. 1(a)], the SrO_2 ought to occur only at the topmost CuO_2 surface of epitaxial SNCO films.

By acquiring bias-dependent STM images with an atomic-scale resolution in Figs. 3(a)–3(d), we further confirm this conclusion for the gridlike superstructure. Intriguingly, the $SrO_2(001)$-$\sqrt{2} \times \sqrt{2}R45^\circ$ surface switches to a $SrO_2(001)$-2×2 structure as the bias polarity is reversed from negative to positive. This suggests that the emergent surface structures, irrespective of $\sqrt{2} \times \sqrt{2}$ and 2×2, may most likely stem from charge ordering in SrO_2 [34,35]. The surface structure switching should be due to a bias-dependent lateral variation of the local density of states in SrO_2 [36], which requires further theoretical investigations. Notwithstanding, the gridlike superstructure remains unchanged in both dimension and orientation. The measured periodicity is 34.7 ± 1.4 Å on average, which is approximately ten times the Sr-Sr atom spacing ($a_{SrO_2} \sim 3.55$ Å) in SrO_2 according to the autocorrelation analysis in Figs. 3(e) and 3(f). Additionally, the possible 2×2 charge ordering of SrO_2 is apparently visible (see the white dashes) in Fig. 3(f), which enables one to deduce the zero angle of the intersection between the respective lattices of SrO_2 and the gridlike superstructure. Note that the latter periodicity of 34.7 ± 1.4 Å coincides nicely with nine times of the lattice constant a_{SNCO} of SNCO films [2,37], a coincidence lattice between the SrO_2 overlayer and CuO_2-terminated SNCO films proposed to be responsible for the gridlike superstructure [Figs. 3(g) and 3(h)]. Figure 3(g) illustrates a simulated moiré pattern by reasonably assuming $a_{SrO_2} = 3.55$ Å and $a_{SNCO} = 3.94$ Å, which matches well our results [Figs. 3(e) and 3(f)].

The coincidence lattice for the superstructure, rather than a simple topographic moiré pattern between the SrO_2 overlayer and underlying CuO_2, is based on two experimental findings. One is the significant dependence of the apparent corrugation of the gridlike superstructure on the applied sample voltage in Figs. 3(a)–3(d). For example, the corrugation of the superstructure is more apparent at negative biases. The other finding relates to the local distortion in the gridlike superstructure and the accompanying charge ordering, which is unexpected for a moiré pattern. Instead, it can be the local structural distortion in the coincidence lattice that yields the bias-dependent corrugation, distorted superstructure, and charge ordering.

Next, we explore the dependence of SNCO films on the nominal composition x of Nd. Five XRD spectra of IL SNCO films at various x are shown in Fig. 4(a). Analogous to La-doped $Sr_{1-x}La_xCuO_2$ (SLCO) IL epitaxial films [8], a second phase with a larger c-axis lattice constant emerges at $x > 0.1$, which coexists and becomes dominant with increasing x. The emergent new phase is characteristic of a $CuO_2(001)$-2×2 surface structure [Fig. 4(b)] and exhibits a hole-doped behavior with the E_F closer to CTB [see the black curve in Fig. 4(c)], which we refer to as p-SNCO. In contrast, the electron-doped n-SNCO films always display a bare $CuO_2(001)$-1×1 surface, even in the two-phase coexisting SNCO films for $x = 0.12$ [Figs. 4(b) and 4(c)]. Without loss of generality, we attribute the $CuO_2(001)$-2×2 surface reconstruction and emergent p-type behavior in SNCO films as the considerable incorporation of apical oxygens in the intervening Sr planes [8], which overwhelms the electron doping by Nd^{3+} donors. In any case, the observed tunneling dI/dV spectra are of striking resemblance, except for an energy shift in E_F. This echoes the self-modulation doping scheme [8], namely, doping the intervening Sr layers changes little the fundamental Mott-Hubbard band structure of $CuO_2(001)$.

Finally, we comment on the implication from the observed SrO_2 overlayers. Based on the step height in Fig. 2(a), we readily estimate the thickness of the SrO_2 overlayer, to wit, only half of a unit cell (~3.3 Å). Evidently, the top SrO_2 layer is insulating and exhibits a large semiconducting gap of ~2.8 eV [Fig. 2(b)]. Notably, the surface stacking of one SrO_2 layer on CuO_2 is structurally similar to the BiO-terminated $Bi_2Sr_2CaCu_2O_{8+\delta}$ [9,10,13], i.e., insulating Sr(Bi) oxides on CuO_2. Here, the measured dI/dV spectra appear sharply different between SrO_2 and CuO_2, and thus how the cuprate database from the vacuum-cleaved BiO planes represents the spectral properties of buried CuO_2 merits further investigations.

The work is financially supported by the Ministry of Science and Technology of China (Grants No. 2017YFA0304600 and No. 2018YFA0305603), the National Natural Science Foundation of China (Grants No. 11774192 and No. 11634007), and in part by Beijing Innovation Center for Future Chips, Tsinghua University.

[1] T. Siegrist, S. M. Zahurak, D. W. Murphy, and R. S. Roth, Nature (London) **334**, 231 (1988).

[2] M. G. Smith, A. Manthiram, J. S. Zhou, J. B. Goodenough, and J. T. Markert, Nature (London) **351**, 549 (1991).

[3] C. T. Chen, P. Seneor, N. C. Yeh, R. P. Vasquez, L. D. Bell, C. U. Jung, J. Y. Kim, M.-S. Park, H.-J. Kim, and S. I. Lee, Phys. Rev. Lett. **88**, 227002 (2002).

[4] N. P. Armitage, P. Fournier, and R. L. Greene, Rev. Mod. Phys. **82**, 2421 (2010).

[5] K. Koguchi, T. Matsumoto, and T. Kawai, Science **267**, 71 (1995).

[6] J. W. Harter, L. Maritato, D. E. Shai, E. J. Monkman, Y. Nie, D. G. Schlom, and K. M. Shen, Phys. Rev. B **92**, 035149 (2015).

[7] Y. Zhong, S. Han, Y. Wang, Z. Luo, D. Zhang, L. Wang, W. Li, K. He, C. L. Song, X. C. Ma, and Q. K. Xue, Phys. Rev. B **97**, 245420 (2018).

[8] Y. Zhong, J.-Q. Fan, R. F. Wang, S. Z. Wang, X. F. Zhang, Y. Y. Zhu, Z. Y. Dou, X.-Q. Yu, Y. Wang, D. Zhang, J. Zhu, C.-L. Song, X.-C. Ma, and Q.-K. Xue, arXiv:1904.12280.

[9] A. Damascelli, Z. Hussain, and Z. X. Shen, Rev. Mod. Phys. **75**, 473 (2003).

[10] Ø. Fischer, M. Kugler, I. Maggio-Aprile, C. Berthod, and C. Renner, Rev. Mod. Phys. **79**, 353 (2007).

[11] C. Ye, P. Cai, R. Yu, X. Zhou, W. Ruan, Q. Liu, C. Jin, and Y. Wang, Nat. Commun. **4**, 1365 (2013).

[12] J. W. Harter, L. Maritato, D. E. Shai, E. J. Monkman, Y. Nie, D. G. Schlom, and K. M. Shen, Phys. Rev. Lett. **109**, 267001 (2012).

[13] S. Misra, S. Oh, D. J. Hornbaker, T. DiLuccio, J. N. Eckstein, and A. Yazdani, Phys. Rev. Lett. **89**, 087002 (2002).

[14] Y. F. Lv, W. L. Wang, J. P. Peng, H. Ding, Y. Wang, L. Wang, K. He, S. H. Ji, R. Zhong, J. Schneeloch, G. D. Gu, C. L. Song, X. C. Ma, and Q. K. Xue, Phys. Rev. Lett. **115**, 237002 (2015).

[15] Y.-F. Lv, W.-L. Wang, H. Ding, Y. Wang, Y. Ding, R. Zhong, J. Schneeloch, G. D. Gu, L. Wang, K. He, S.-H. Ji, L. Zhao, X.-J. Zhou, C.-L. Song, X.-C. Ma, and Q.-K. Xue, Phys. Rev. B **93**, 140504(R) (2016).

[16] Y. Zhong, Y. Wang, S. Han, Y. F. Lv, W. L. Wang, D. Zhang, H. Ding, Y. M. Zhang, L. Wang, K. He, R. D. Zhong, J. A. Schneeloch, G. D. Gu, C. L. Song, X. C. Ma, and Q. K. Xue, Sci. Bull. **61**, 1239 (2016).

[17] M. Takano, Y. Takeda, H. Okada, M. Miyamoto, and T. Kusaka, Physica C **159**, 375 (1989).

[18] G. Er, S. Kikkawa, and F. Kanamaru, Physica C **235**, 983 (1994).

[19] A. Gupta, B. Mercey, H. Hervieu, and B. Raveau, Chem. Mater. **6**, 1011 (1994).

[20] V. Leca, D. H. A. Blank, G. Rijnders, S. Bals, and G. Van Tendeloo, Appl. Phys. Lett. **89**, 092504 (2006).

[21] J. Tomaschko, V. Leca, T. Selistrovski, S. Diebold, J. Jochum, R. Kleiner, and D. Koelle, Phys. Rev. B **85**, 024519 (2012).

[22] S.-i. Karimoto, K. Ueda, M. Naito, and T. Imai, Appl. Phys. Lett. **79**, 2767 (2001).

[23] Y. Krockenberger and H. Yamamoto, Physica C **471**, 185 (2011).

[24] Y. Krockenberger, K. Sakuma, and H. Yamamoto, Appl. Phys. Express **5**, 043101 (2012).

[25] A. Ikeda, Y. Krockenberger, and H. Yamamoto, Phys. Rev. Materials **3**, 064803 (2019).

[26] Y. Krockenberger, A. Ikeda, K. Kumakura, and H. Yamamoto, J. Appl. Phys. **124**, 073905 (2018).

[27] Y. Matsushita, Y. Oyama, M. Hasegawa, and H. Takei, J. Solid State Chem. **114**, 289 (1995).

[28] N. C. Hyatt, L. Gray, I. Gameson, P. P. Edwards, and S. Hull, Phys. Rev. B **70**, 214101 (2004).

[29] P. Abbamonte, G. Blumberg, A. Rusydi, A. Gozar, P. Evans, T. Siegrist, L. Venema, H. Eisaki, E. D. Isaacs, and G. A. Sawatzky, Nature (London) **431**, 1078 (2004).

[30] S. C. Middleburgh, K. P. D. Lagerlof, and R. W. Grimes, J. Am. Ceram. Soc. **96**, 308 (2013).

[31] C. N. Mihailescu, I. Pasuk, M. Straticiuc, C. R. Nita, D. Pantelica, and J. Giapintzakis, Appl. Surf. Sci. **320**, 852 (2014).

[32] Y. Y. Li, G. Wang, X. G. Zhu, M. H. Liu, C. Ye, X. Chen, Y. Y. Wang, K. He, L. L. Wang, X. C. Ma, H. J. Zhang, X. Dia, Z. Fang, X. C. Xie, Y. Liu, X. L. Qi, J. F. Jia, S. C. Zhang, and Q. K. Xue, Adv. Mater. **22**, 4002 (2010).

[33] C.-L. Song, Y.-L. Wang, Y.-P. Jiang, Z. Li, L. Wang, K. He, X. Chen, X.-C. Ma, and Q.-K. Xue, Phys. Rev. B **84**, 020503(R) (2011).

[34] C. Renner, G. Aeppli, B.-G. Kim, Y.-A. Soh, and S.-W. Cheong, Nature (London) **416**, 518 (2002).

[35] K. Iwaya, R. Shimizu, T. Ohsawa, T. Hashizume, and T. Hitosugi, Phys. Rev. B **83**, 125117 (2011).

[36] T. Maroutian, S. Degen, C. Becker, K. Wandelt, and R. Berndt, Phys. Rev. B **68**, 155414 (2003).

[37] V. Bobrovskii, A. Mirmelstein, A. Podlesnyak, I. Zhdakhin, B. Goshchitskii, E. Mitberg, V. Zubkov, T. D'yachkova, N. Kadyrova, E. Khlybov, F. Fauth, and A. Furrer, Physica B **234**, 818 (1997).